PNAS
www.pnas.org

Supplementary Information for

Structural titration of receptor ion channel GLIC gating by HS-AFM

Authors: Yi Ruan[†,‡] , Kevin Kao[#,¶], Solène Lefebvre[††], Arin Marchesi[‡], Pierre-Jean Corringer[††], Richard K Hite[#] & Simon Scheuring[‡,‡‡, §§,*]
Affiliations:
† Collaborative Innovation Center for Bio-Med Physics Information Technology(CICBMPIT), College of Science, Zhejiang University of Technology, 310023 Hangzhou, China.
‡ U1006 Institut National de la Santé Et Recherche Médicale (INSERM), Université Aix-Marseille, Parc Scientifique et Technologique de Luminy, 13009 Marseille, France.
# Structural Biology Program, Memorial Sloan Kettering Cancer Center, 1275 York Ave, New York 10065 NY, USA.
¶Weill Cornell/Rockefeller/Sloan Kettering Tri-Institutional MD-PhD Program, New York 10065 NY, USA.
†† Channel-Receptors Unit, Institut Pasteur, CNRS UMR 3571, 75015 Paris, France
‡‡ Department of Anesthesiology, Weill Cornell Medicine, 1300 York Avenue, New York, 10065 NY, USA.
§§ Department of Physiology and Biophysics, Weill Cornell Medicine, 1300 York Avenue, New York, 10065 NY, USA.

* Correspondence to: S. Scheuring, email: sis2019@med.cornell.edu

This PDF file includes:

Supplementary information Text
Figs. S1 to S7
Captions for movies S1 to S4
References for SI reference citations

Other supplementary materials for this manuscript include the following:

Movies S1 to S4

Supplementary Information Text:

Similarity between open and closed GLIC X-ray structures:

We assessed the similarity of the acidic pH open (PDB 3EAM)(1) and neutral pH closed (PDB 4NPQ)(2) GLIC X-ray structures through alignment and calculation of the root mean square (rms) deviation of the atomic coordiantes in PyMol. After 5 cycles of alignments 1372 atoms had an rms of 2.472Å.

Fig. S1.

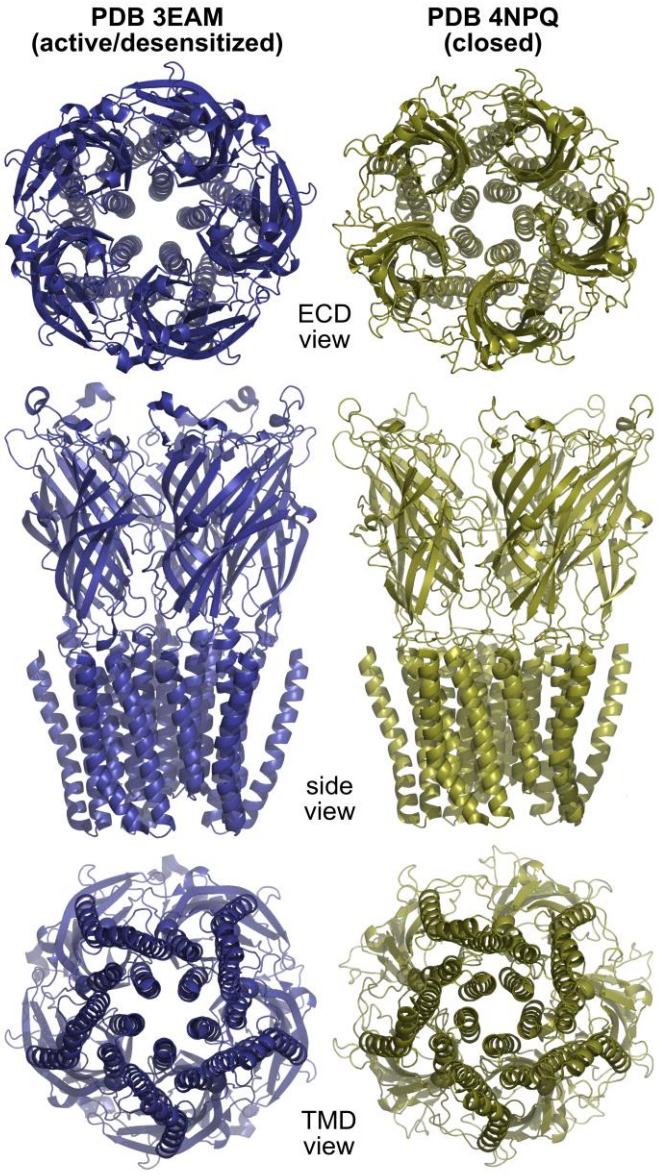

Fig. S1. Comparison of active/desensitized **and closed GLIC X-ray structures**. Left, crystal structure of GLIC in the active/desensitized state (PDB 3EAM, blue). Right, crystal structure of GLIC in the closed state (PDB 4NPQ, yellow). Top: view from the extracellular face onto the ECDs. Middle: side view in the membrane plane. Bottom: view from the intracellular face onto the TMDs. The pore-lining helices (M2) are more constricted in the closed structure, yet the overall conformational differences between the two structures are minor.

Fig. S2.

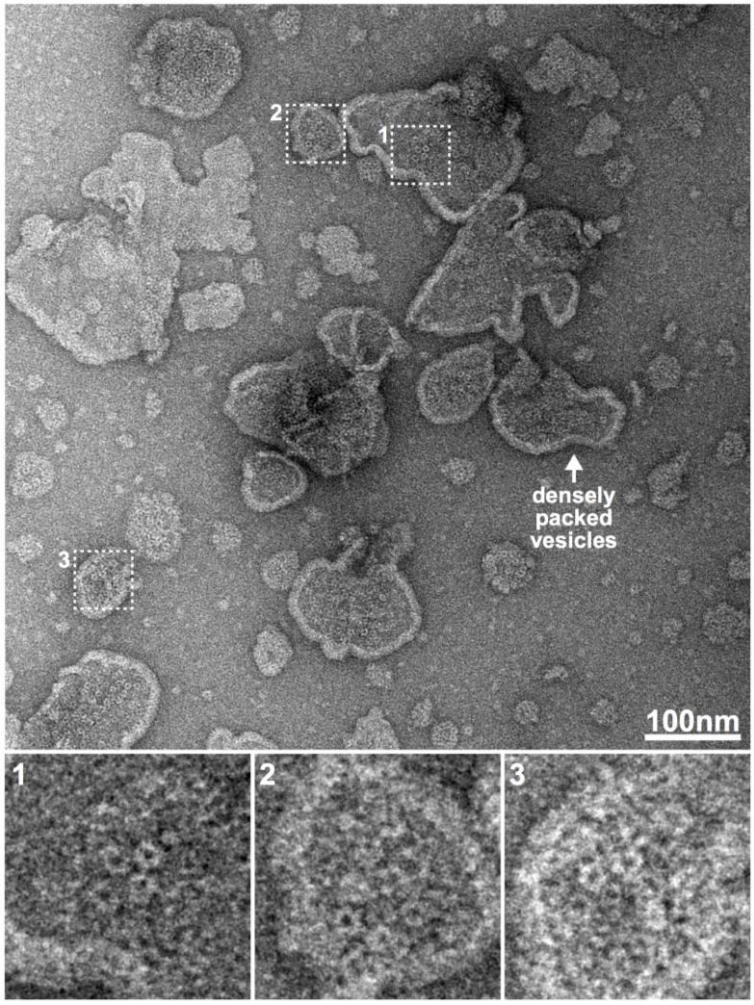

Fig. S2. Reconstitution of GLIC in large densely packed vesicles. During reconstitution, the solubilized protein was mixed with solubilized lipids at lipid-to-protein ratios (w/w) ~1 followed by detergent removal using Biobeads. After reconstitution, vesicles were checked using negative stain electron microscopy (top panel). The dashed squares outline the image areas displayed in the bottom inset panels, displaying the reconstitution of flower-shaped proteins with size corresponding to GLIC channels.

Fig. S3.

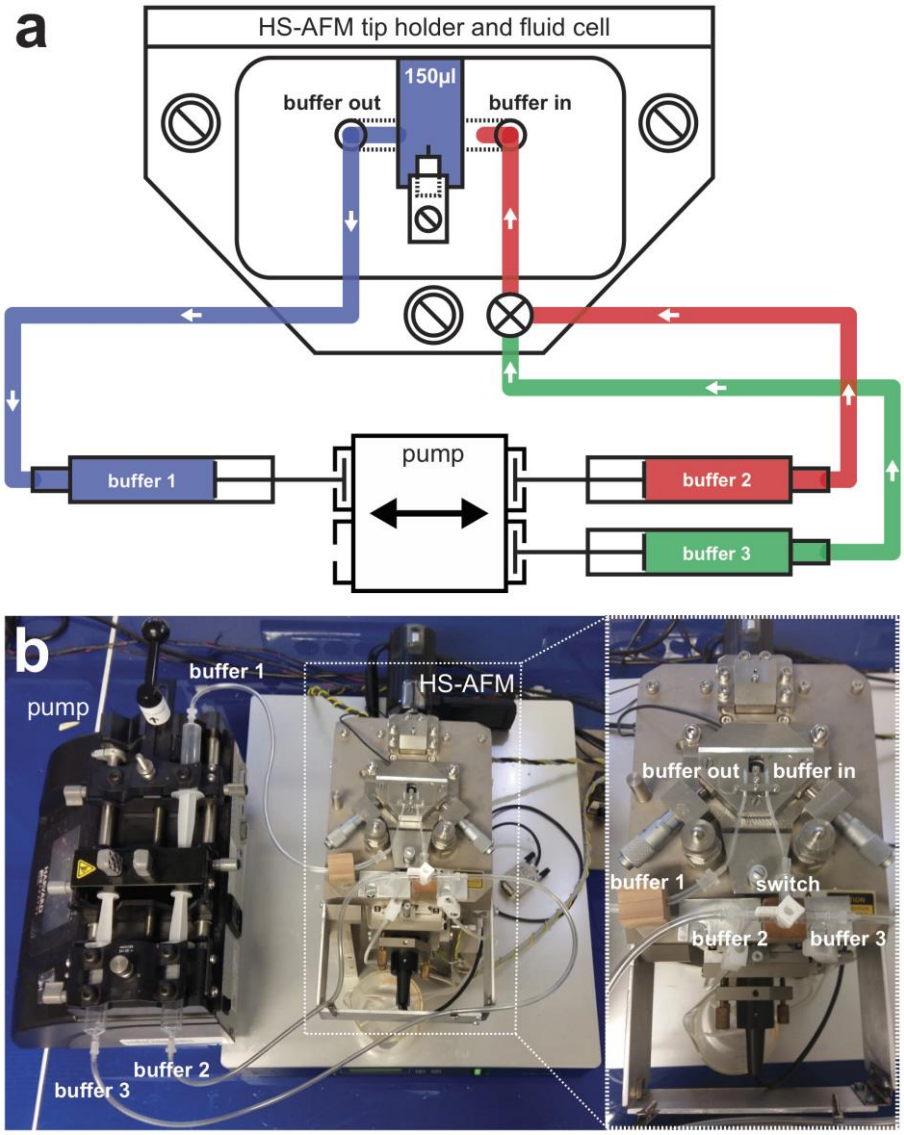

Fig. S3. High precision buffer exchange system coupled to HS-AFM. a) Schematic representation of the coupling of the buffer exchange system to the HS-AFM fluid cell. The 'buffer in' and 'buffer out' channels are placed in proximity to the HS-AFM cantilever (central element inside the fluid cell). The fluid cell contains initially 150ul of buffer 1 (blue) that is connected to the receiving syringe. Buffer 2 (red) is the first buffer to be injected into the fluid cell. Note the slight gap between buffer 2 and the fluid cell, representing a tiny bubble in the tubing to avoid involuntary mixing of buffer 2 before activation of the pumping system. By the use of a switch in the tubing system, buffer 3 (green) can later be injected into the fluid cell. Buffer 3 can be identical to buffer 1, allowing for a reversibility experiment. **b**) Photographs of HS-AFM setup coupled to the buffer exchange system. The same elements are labeled as in a) where possible.

Supplementary Information Text:

Thoughts about repetitive 2D-patterns containing molecules with 5-fold symmetry:

Membrane proteins are structurally restricted to the membrane plane. With the rare exceptions where membrane proteins form regular helical membrane tubules(3), the membranes remain planar and the membrane proteins in can form regular 2D-crystals(4). 2D symmetry space groups, *aka* plane symmetry groups or wallpaper groups, can only occur in 17 flavors, and can be subdivided into *p*1, *p*2, *p*3, *p*4 and *p*6 symmetry group families, depending if they display none, a 2-fold, 3-fold, 4-fold or 6-fold symmetry axis(5). Often, the 2D space group in which a membrane protein forms 2D-crystals is related to its internal symmetry/stoichiometry, *eg.* the p2 2Dcrystals of dimeric NhaA(6), the *p*3 2D-crystals of trimeric bacteriorhodopsin(7), the *p*4 2D-crystals of tetrameric AQP0(8), and the *p*6 2D-crystals of hexameric gap junction connexons(9). In contrast 5-fold symmetry is incompatible with regular 2D unit cell propagation and *p*5 symmetry space groups do not exist.

Having detected visually the surprising patterns comprising a large number of GLIC channels (**Figure S4a**, see **Figure 2c** in the main manuscript), we set out to proof that we are indeed looking at higher-order organization of the channels. Given that no *p*5 symmetry space group exists, we had to look out for other geometrical patterns, and visually associated the found GLIC patterns with medieval quasi-crystalline tiling in Islamic architecture that have been shown to antecede the today better known Penrose patterns(10). In such tiling pentagons are symmetry related and propagated to form long-range regular patterns comprising pentagons (**Figure S4c, yellow outline**), and some of these patterns described well the association of GLICs in the membrane (**Figure S4b, yellow outline**). We elaborated the geometrical operations to form such patterns(11, 12), and adapted them to our case, which resulted in a pattern of 19 pentagons (**Figure S4d, bottom left**). This pattern suggested that the entire assembly of GLICs could be 6-fold symmetrized and, with the exception of the central molecule, all GLICs should find symmetry mates with subunit precision. This was indeed the case: applying 6-fold symmetry to the assembly image in (**Figure 2c, bottom)** results in a highly contrasted pattern of GLIC pentamers with resolved subunit orientation (**Figure S4a**), meaning that the angular orientation of all molecules in the pattern is defined. The pattern of the 19 GLIC pentamers (**Figure 2c, Figure S4b**) has six *p*3 axis, six *p*2 axis and one *p*6 axis centers. Interestingly applying the *p*6 operation on the central molecule made us realize that there were another 6 highly conserved pentamers at the periphery of the assembly (**Figure S4b, arrows**). These molecules are symmetry-related (over the *p*2 axes) with the central molecule, and thus suggest that the pattern can be entirely propagated (**Figure S4d, bottom right**). The result shows that the minimal unit to construct such regular patterns of pentamers is a trimer of pentamers (see mixed color elements between the yellow, blue and red patterns).

In summary, we detected in the membrane a regular assembly of 19 GLICs that allow 18 of 19 channels to partner with 5 neighbors in a predictable and regular manner. The trimer of pentamers is the minimal assembly unit. With this knowledge at hand, one can see many *p*3 trimers-of-pentamers and *p*2 tetramers-of-pentamers in **Figures 1c-f, first column**.

We conclude that despite the incompatibility of a 5-fold symmetrical molecule with a plane symmetry group, the open conformation GLICs ‘force’ association with five neighbors, signature of specific and strong intermolecular interactions.

Fig. S4.

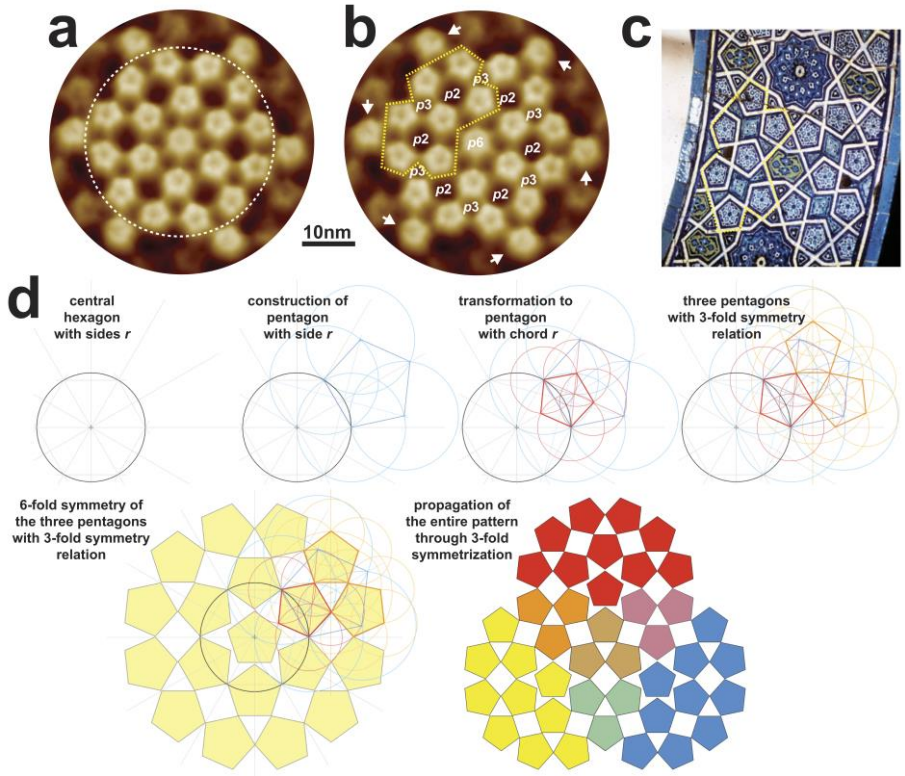

Fig. S4. Open conformation GLICs engage into intricate supramolecular organisations with specific protein-protein interactions. a) 6-fold symmetrized GLIC assembly of the membrane organization imaged in Figure 1f, right, the dashed circle surround the assembly outlined in Figure 2c, bottom. **b)** Assembly shown in a) with internal *p*6, *p*3 and *p*2 centers indicated. Yellow outline: Assembly of 7 pentamers that reminded is of medieval Islamic pentagonal patterns. **c)** Interior archway at the opening of the Sultan's Lodge in the Ottoman Green Mosque in Bursa, Turkey (1424), with pentagons (this image is in the public domain in its country of origin and other countries and areas where the copyright term is the author's life plus 100 years or less). The yellow outline highlights a pattern of pentagons that are reminiscent of the GLIC assembly in b). **d)** Steps 1-4: construction of a pattern similar to the one shown in c) based on reference(12) with adaptations. Step 5 (bottom left): 6-fold symmetry results in a pattern strongly reminiscent to the patern found in the GLIC membrane (Figure 1f and 2c). Step 6 (bottom right): Based on the finding in the GLIC membrane that additional 6 channels surrounded the assembly of 19 channels in a regular way as symmetry mates of the central molecule of this assembly, we propagated the entire pattern accordingly (blue and red assembly). This overlay indicated that the trimer-of-pentamer was the minimal unit from which these intricate assemblies are built (see mixed color trimers of pentamers at the interfaces of / part of two neighboring 19-channels assemblies.

Fig. S5.

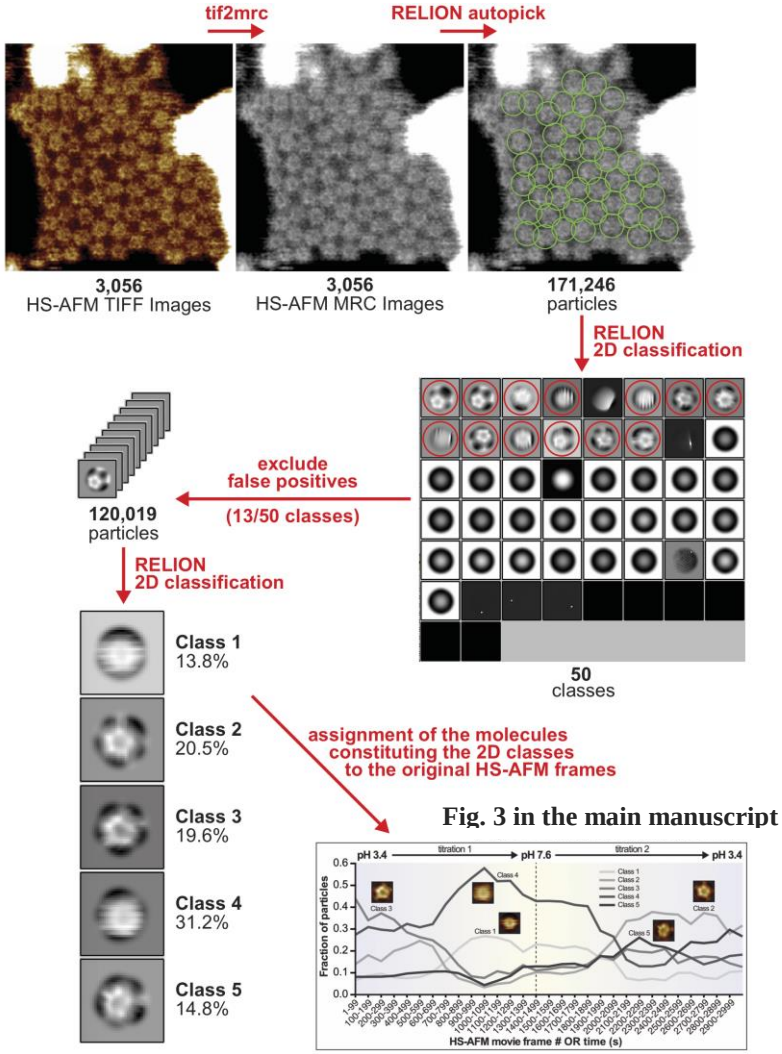

Fig. S5. Processing workflow for reference-free class averaging and molecule reassignment for the pH titration experiment. Processing steps are indicated by red arrows and labeled according to the undertaken procedure (from top left to bottom right). A HS-AFM movie is separated into 3,056 individual 32bit TIFF format images. Using tif2mrc the images are converted to 3,056 16bit MRC format images. 171,246 channel images were automatically selected from these images using the autopick command in RELION. Particle picking was checked by visual inspection. Reference-free 2D classification of the channel images was used to eliminate false positives from the data set. Of the 50 specified classes, 13 class averages displayed features consistent with GLIC while the particle images comprising the remaining 37 averages were considered to be false-positives (saturated image areas and noise). The 120,019 particles from the 13 selected classes are pooled and subjected to a second cycle of RELION 2D classification specifying 5 classes. Finally, the molecules comprising each class are reassigned to their HS-AFM frame of origin and the fraction of particles representing each class are pooled within bins of 100 subsequent image frames to result in the structural titration experiment plot (see Figure 3 in the main manuscript).

Fig. S6.

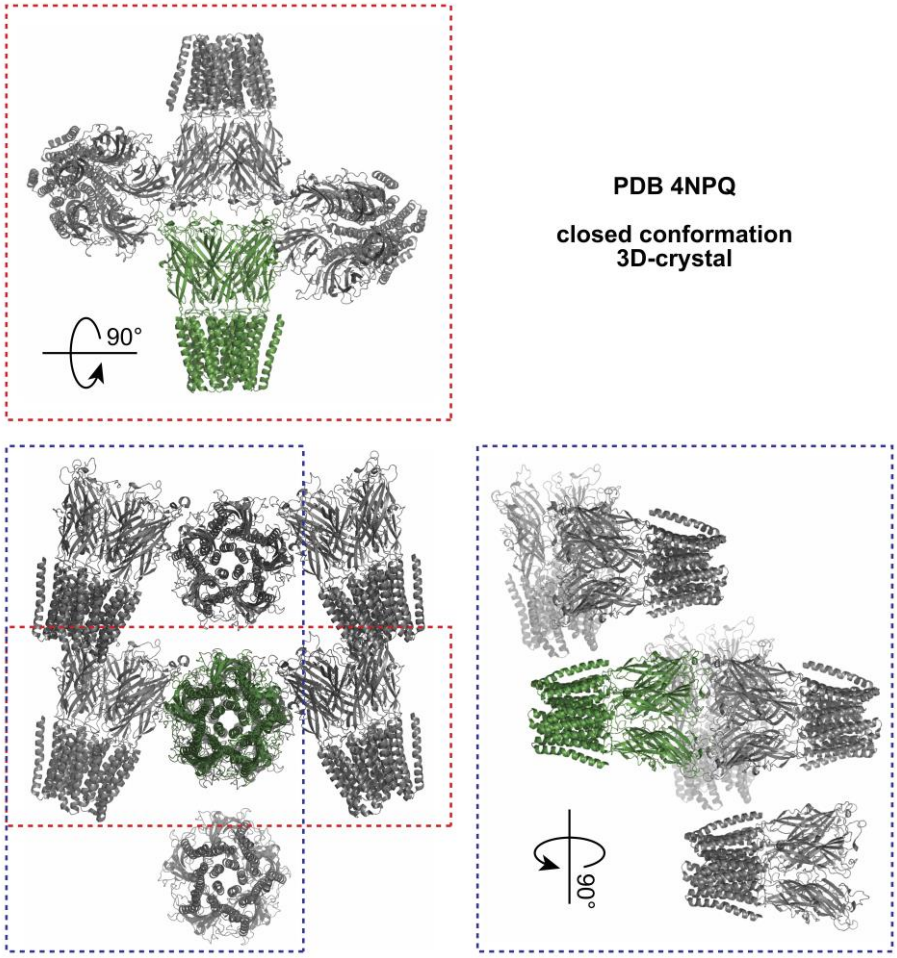

Fig. S6. Extensive protein-protein contacts in the 3D-crystals used for GLIC X-ray structure determination of the closed state. Bottom left: 2 unit cells of the crystal packing of GLIC in a closed state (PDB 4NPQ, green). One molecule is highlighted by coloring while the neighboring molecules are shown in teal. The ECDs undergo extensive head-to-head association with one (top and right) and peripheral interactions with ECDs from two more channels (top). An antiparallel arranged channel from the neighboring unit cell lines the highlighted molecule (right).

Fig. S7.

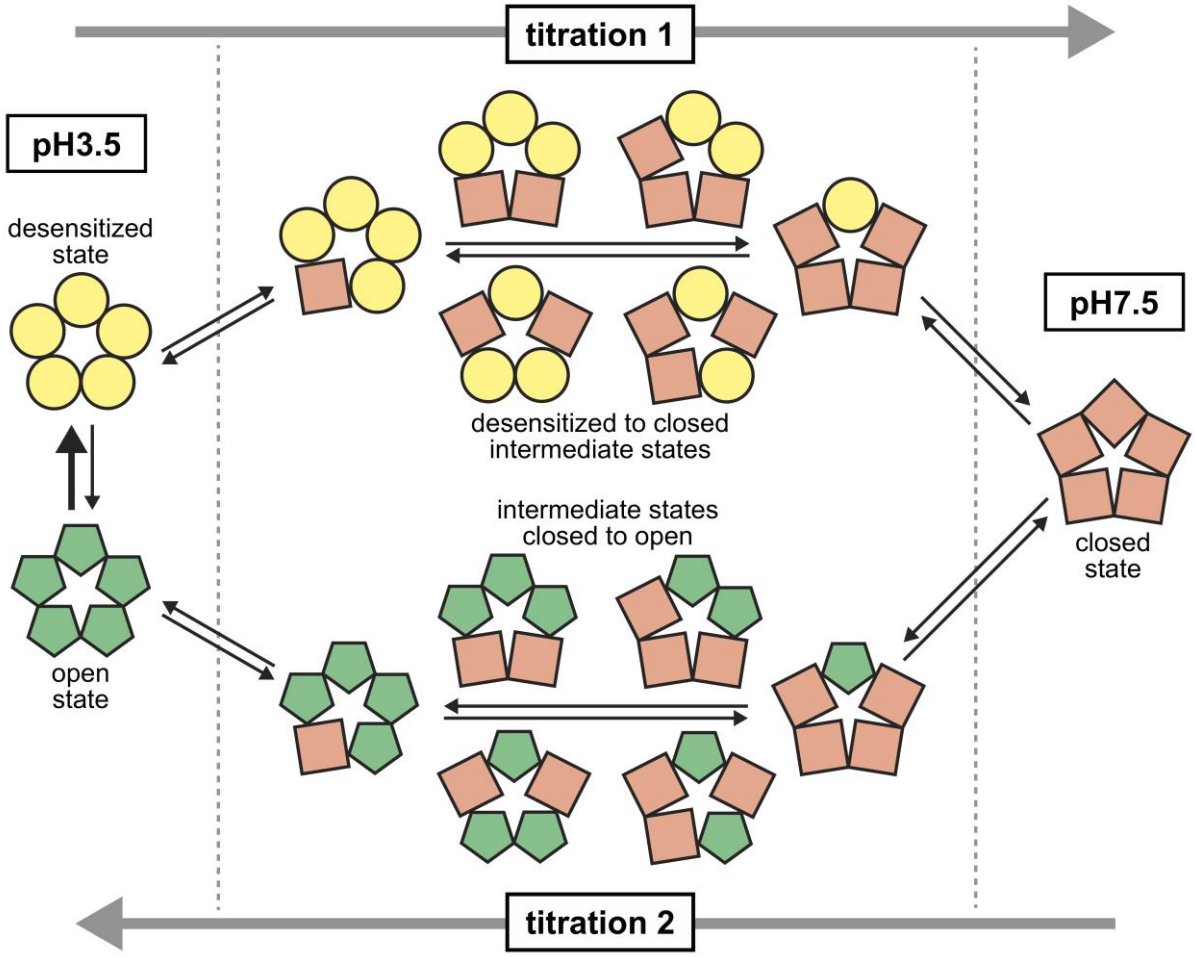

Fig. S7. State transition model of GLIC during the titration experiment. The structural titration experiments in the HS-AFM may reveal the presence of multiple states during the open to closed and closed to desensitized states transitions. Given prolonged exposure of the channels to acidic pH prior to imaging, the initial state of all channels should be the functionally desensitized state. The first titration experiment will transform the desensitized state into the closed state at physiological pH. The second titration will activate the oligomeric channel, potentially not in a fully concerted manner, to reach the short-lived open state that will desensitize again upon prolonged exposure to low pH.

Captions for movies S1 to S4 :

Movie S1. GLIC structural titration from pH3.4 to pH7.5 monitored by high-speed atomic force microscopy (HS-AFM). Left: Drift-corrected HS-AFM movie recorded at 80nm x 80nm image size and 1 frame per second imaging speed. The fluid chamber contained ~150 µL and the buffer exchange rate was 5 µL/min. Right: Running average over 3 consecutive frames (3s) of the movie shown on the left.

Movie S2. GLIC structural titration from pH3.4 to pH7.5 monitored by high-speed atomic force microscopy (HS-AFM). Left: Drift-corrected HS-AFM movie recorded at 80nm x 80nm image size and 1 frame per second imaging speed. The fluid chamber contained ~150 µL and the buffer exchange rate was 5 µL/min. Right: Running average over 3 consecutive frames (3s) of the movie shown on the left.

Movie S3. GLIC structural titrations from pH3.4 to pH7.5 and from pH7.5 to pH3.4 monitored by high-speed atomic force microscopy (HS-AFM). Left: Drift-corrected HS-AFM movie recorded at 80nm x 80nm image size and 1 frame per second imaging speed. The fluid chamber contained ~150 µL and the buffer exchange rate was 10 µL/min. Right: Running average over 3 consecutive frames (3s) of the movie shown on the left.

Movie S4. GLIC structural titrations from pH3.4 to pH7.5 and from pH7.5 to pH3.4 monitored by high-speed atomic force microscopy (HS-AFM). Left: Drift-corrected HS-AFM movie recorded at 80nm x 80nm image size and 1 frame per second imaging speed. The fluid chamber contained ~150 µL and the buffer exchange rate was 15 µL/min. Right: Running average over 3 consecutive frames (3s) of the movie shown on the left.

References:

1. Bocquet N*, et al.* (2009) X-ray structure of a pentameric ligand-gated ion channel in an apparently open conformation. *Nature* 457(7225):111-114.
2. Sauguet L*, et al.* (2014) Crystal structures of a pentameric ligand-gated ion channel provide a mechanism for activation. *Proceedings of the National Academy of Sciences of the United States of America* 111(3):966-971.
3. Miyazawa A, Fujiyoshi Y, & Unwin N (2003) Structure and gating mechanism of the acetylcholine receptor pore. *Nature* 423(6943):949-955.
4. Stahlberg H*, et al.* (2001) Two-dimensional crystals: a powerful approach to assess structure, function and dynamics of membrane proteins. *Febs Letters* 504(3):166-172.
5. Crowther RA, Henderson R, & Smith JM (1996) MRC image processing programs. *J. Struct. Biol.* 116:9-16.
6. Williams KA (2000) Three-dimensional structure of the ion-coupled transport protein NhaA. *Nature* 403:112.
7. Unwin PNT & Henderson R (1975) Molecular Structure Determination by Electron Microscopy of Unstained Crystalline Specimens. *J. Mol. Biol.* 94:425-440.
8. Gonen T*, et al.* (2005) Lipid–protein interactions in double-layered two-dimensional AQP0 crystals. *Nature* 438:633.
9. Unger VM, Kumar NM, Gilula NB, & Yeager M (1999) Three-Dimensional Structure of a Recombinant Gap Junction Membrane Channel. *Science* 283(5405):1176.
10. Lu PJ & Steinhardt PJ (2007) Decagonal and Quasi-Crystalline Tilings in Medieval Islamic Architecture. *Science* 315(5815):1106.
11. Abdullahi Y & Embi MRB (2013) Evolution of Islamic geometric patterns. *Frontiers of Architectural Research* 2(2):243-251.
12. Dabbour LM (2012) Geometric proportions: The underlying structure of design process for Islamic geometric patterns. *Frontiers of Architectural Research* 1(4):380-391.